Vietnam Journal of Catalysis and Adsorption
Tạp chí xúc tác và hấp phụ Việt Nam

http://jca.edu.vn

Direct synthesis of Cu-TiO_2-SBA-16 photocatalysts and its application for the oxidative desulfurization of fuel oil model

Truong Thi Hanh[1], Vu Duc Cuong[2], Pham Xuan Nui[3,*]

[1] *Institute of Environment, Vietnam Maritime University, 484 Lach Tray, Kenh Duong, Le Chan, Hai Phong, Vietnam.*
[2] *Viet Tri University of Industry, 9-Tien Son, Tien Cat, Viet Tri, Phu Tho, Vietnam.*
[3] *Department of Chemical Engineering, Hanoi University of Mining and Geology, 18 Pho Vien, Duc Thang, Bac Tu Liem, Hanoi, Vietnam.*
**Email: phamxuannui@humg.edu.vn*

ARTICLE INFO

Received: 05/08/2024
Accepted: 13/09/2024
Published: 30/09/2024

Keywords:
SBA-16; TiO_2; photocatalytic; oxidative desulfurization (ODS); dibenzothiophene (DBT)

ABSTRACT

In this study, the Cu-TiO_2-SBA-16 photocatalytic materials were successfully prepared by direct hydrothermal synthesis method. The products were characterized by X-ray diffraction (XRD), Ultraviolet–Visible Diffuse Reflectance Spectroscopy (UV-Vis DRS), energy dispersive X-ray (EDX), transmission electron microscopy (TEM), N_2 adsorption–desorption isotherms, X-ray photoelectron spectroscopy (XPS) methods. The analysis illustrated that Cu-TiO_2 nanocrystals were successfully incorporated into the SBA-16 mesopores. The photocatalytic activity of these Cu-TiO_2-SBA-16 mesoporous materials have been tested by the oxidative desulfurization reaction of dibenzothiophene (DBT) using H_2O_2 as an oxidant under UV light irradiation. The results showed that the Cu-TiO_2-SBA-16 mesoporous materials prepared at the Cu/Ti mole ratios of 0.05 showed higher photocatalytic activity than the rest due to the decrease in band gap energy.

1. Introduction

Sulfur compounds in fuel oils lead to the emission of sulfur oxide gases (SOx) which causes equipment corrosion and respiratory disorders in humans, acidifies soil and damages forests and various other ecosystems [1]. Furthermore, the presence of sulfur compounds during the refining process can promote the poisoning of some catalysts and cause corrosion problems in pipelines, pumping and refining equipment [2,3]. To reduce SOx emissions, many countries around the world have introduced stricter requirements on the sulfur content of raw materials [4]. Therefore, deep desulfurization of fuel oils has attracted increasing attention worldwide. The conventional method for removing sulfur is to use hydrodesulphurization (HDS). This method requires to be carried out under harsh conditions such as high temperature and pressure (300 - 340°C, 20 -100 atm) and high hydrogen pressures [5]. Although HDS is highly efficient in removing thiols, sulfides, and disulfides, this method still encounters many difficulties when desulfurizing aromatic sulfur compounds such as dibenzothiophene (DBT), benzothiophene (BT), and derivatives [6]. To overcome these problems, many methods have been applied such as oxidation and reduction of sulfur, adsorption and desulfurization, extraction with ionic liquid, biological desulfurization [7],... The catalytic oxidative

https://doi.org/10.62239/jca.2024.055

desulfurization sulfur (ODS) method is one of the methods that has the potential to replace the HDS method due to mild operating conditions such as low temperature, pressure and no hydrogen consumption [8]. Under these conditions, sulfur-containing compounds can be selectively oxidized to sulfoxides or sulfones in the presence of hydrogen peroxide. There are many catalysts that have been studied for use in the ODS process such as ionic liquids, polyoxometalates [9],...

In recent years, there have been many studies on TiO_2 due to its good photocatalytic properties and low price. Some studies have aimed to improve the catalytic properties and expand the light absorption ability of TiO_2 to the visible light region by doping many metals such as Ni, Fe, Sn and Cu [10,11]. Copper has been investigated as a dopant, and copper oxide (CuO) illustrated a high absorption coefficient due to its narrow band gap of 1.2 eV. CuO modified TiO_2 demonstrated the highest photocatalytic activity in comparison with other metals [12], Besides, TiO_2 catalyst based on anderson-polyoxometalates [21], TiO_2-Modified Y Zeolite [22] using for photocatalytic oxidative desulfurization under visible light. TiO_2 and Cu-TiO_2 can be synthesized by many techniques. Among the above methods, the sol-gel method has many advantages such as high purity and compositional homogeneity of the products [13].

Although the nanosynthesis of TiO_2 and modified TiO_2 is well established, there are still some problems that still generally exist during production. For example, TiO_2 usually consists of tiny particles , which are difficult and expensive to separate and recover from suspension after regeneration, especially when it coexists with multicharged ions. In addition, TiO_2 nanoparticles easily agglomerate into larger particles and reduce catalytic efficiency [14]. To overcome this drawback, some studies have attached TiO_2 to supports such as zeolite, MCM-41 as well as many other mesoporous SBA-15 with with channel-like pore structures and high specific surface area, have been considered as prospective materials in catalysis [15,16]. Among these silica materials, SBA-16 is considered a very interesting mesostructure due to the fact it has a three-dimensional (3-D) cage-like mesostructure, corresponding to the *Im3m* space group [17]. Up to now, there have not been many published results of incorporating metal ions into the SBA-16 framework for the sulfur redox process.

In this study, Cu-TiO_2 nanocrystals were synthesized by the sol-gel method through a precursor solution of titanium isopropoxide and copper acetate. Then, the Cu-TiO_2 sol was used as the metal source in the direct synthesis of SBA-16 material. The synthesized catalysts were studied for their structural and optical properties. The photocatalytic activity of photocatalysts in the decomposition of dibenzothiophene under UV irradiation was also studied.

2. Experimental

Materials

Pluronic F127 ($EO_{106}PO_{70}EO_{106}$), tetraethyl orthosilicate (TEOS), chlorhydric acid (HCl), n-butanol (C_4H_9OH), titanium isopropoxide ($Ti(OC_3H_7)_4$), ethanol (C_2H_5OH), acetic acid (CH_3COOH), acetate copper $(CH_3COO)_2Cu$, dibenzothiophene (DBT), hydrogen peroxide (H_2O_2) were purchased from Sigma-Aldrich, Merck and Xilong companies.

Preparation of photocatalyst

Initially, Cu-TiO_2 nanocrystals were prepared by the sol-gel method: Briefly, a mixture containing 0.36 mL of acetic acid CH_3COOH and 3.6 mL of ethanol was stirred for 15 minutes. After that, 0.1 mL of titanium (IV) isopropoxide $(Ti(OC_3H_7)_4$ was added to this solution then continuously stirred for 30 minutes to obtain TiO_2 nanocrystals. x Cu-TiO_2 crystals (x=0%, 5%, 10% and 15%) were synthesized by adding a solution of acetate copper $(CH_3COO)_2Cu$ with different content of 5 mL ethanol into the TiO_2 nanocrystal solution and stirring for 2 h.

SBA-16 was synthesized by hydrothermal method from the TEOS and F127 as precursors: 1 g of F127 was dissolved in 50 mL of distilled water. After 1 h of stirring, 5.5 mL of 12 M HCl was added, stirring continuously for 2 h at room temperature to obtain the homogenous mixture. Then, 3.7 mL of *n*-butanol was added to the mixture, Finally, 5.3 mL of TEOS was added slowly to yield a gel mixture, continuously stirring at 40 °C for 24 h. The mixture was then placed under a static condition at 100 °C for another 24 h in an autoclave. The precipitated solid product was separated by filtration and washed with distilled water and ethanol, then dried at 100 °C and then calcined at 550 °C for 6 h to obtain the SBA-16 powder.

Preparation of Cu-TiO_2-SBA-16: Cu-TiO_2 sol was added to the mixture of F127, HCl and *n*-butanol in the above process. After adding Cu-TiO_2 sol, the mixture was maintained at 40 °C for 6 h so that the Cu-TiO_2 nanocrystals attach and distributed evenly in the block structure of SBA-16. The next steps are the same as the

https://doi.org/10.62239/jca.2024.055

above process, finally obtaining xCu-TiO_2-SBA-16 material (x=0%, 5%, 10%, 15%).

Characterization

Powder X-ray diffraction patterns were recorded on a D8-Advance Bruker with Cu-Kα radiation (λ=1.5406 nm). BET surface areas were calculated using N_2 at 77 K with P/P_o between 0.05 and 0.3. Pore size distributions were calculated from the N_2 isotherms using the the Barret-Joyner-Halenda (BJH) model. Energy-dispersive X-ray spectroscopy analysis (EDX) was measured on a JED-2300 with gold coating. The images of TEM were taken by a Jeol JEM-1010 with an accelerating voltage of 200 kV. XPS spectra were taken on an ESCALab 250 spectrometer using monochromated Al Kα radiation (1486.6 eV).

Photocatalytic activity test

The photocatalytic activity was evaluated by measuring the conversion of a DBT solution (containing 600 ppm sulfur) in *n*-octane with the presence of the prepared catalyst under UV irradiation. In this experiment, 0.15 g of photocatalyst and 20 mL of DBT solution were added into a 150 mL three-necked round bottom flask with water condenser, then the mixture was stirred for 1 hour in the dark to achieve adsorption and adsorption balance. Then, the amount of hydrogen peroxide was dropped into the flask and the mixture was then exposed to UV light (35 W) while stirring at temperatures of 70 °C. Reaction solution samples were collected every 1 h for 5 h. The catalyst is separated from the sample solution by a filter. The remaining DBT content was determined by HPLC analysis method Shimadzu HPLC Series 20A Waters X-Bridge C18 column (25 cm x 4 mm x 5 µm).

3. Results and discussion

X-ray diffraction characterization

In Fig. 1A, all XRD patterns performed at low angle showed three diffraction peaks (2θ ≈ 0.72°, 0.96°, and 1.32°) related to (110), (200) and (211) reflections were shown, respectively. These peaks can be assigned to an ordered, three-dimensional, mesoporous, cubic Im3m structure of SBA-16 [17], which indicate that the preparation method performed in this study did not destroy the structure of SBA-16.

The wide-angle XRD patterns showed that typical broad diffraction peaks are around 2θ≈24° which is characteristic of the amorphous silica structure. There are no clear characteristic peaks of crystalline metal oxides in XRD patterns of samples, which indicates that crystalline metal oxides were not formed on the surface of materials perhaps due to the incorporation of metal oxide nanocrystals into the silica framework.

Fig. 1B shows the UV-vis diffuse reflectance spectra of all samples. It can be seen that all Ti-containing samples have absorption bands in the UV-vis region. The samples showed an intense band centered at about 220 nm which is assigned to the mono-atomically dispersed Ti^{4+} ions in tetra-coordinated geometry [18]. This result suggests that Ti^{4+} ions are successfully incorporated into the framework of SBA-16.

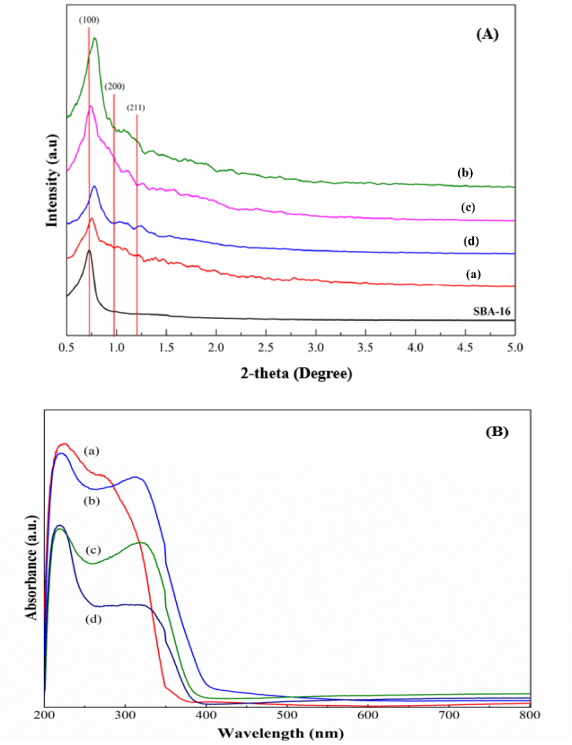

Fig. 1: (A) Low- angle XRD patterns of the synthesized materials; (B) UV-Vis-DRS spectra of (a) TiO_2-SBA-16, (b) 5%Cu-TiO_2-SBA-16, (c) 10%Cu-TiO_2-SBA-16, (d) 15%Cu-TiO_2-SBA-16.

UV-Vis-DRS spectrum of synthesized samples

Gap band energy (E_{gap}) was calculated from UV-Vis spectra. Egap value of Ti-containing SBA-16 is lower in presence of Cu (3.20 eV versus 2.95, 3.10, 3.12 eV corresponding to different Cu content) which indicates that modifying TiO_2 with Cu is effective in decreasing the E_{gap} of Ti-containing SBA-16 material. In addition, when the Cu content was increased in TiO_2-containing SBA-16, the E_{gap} values decreased. E_{gap} values of 5, 10 and 15%Cu-TiO_2-SBA-16 are 2.95, 3.10 and 3.12 eV, respectively. This is due to the crystallization of CuO preventing the light absorption ability of material. The

https://doi.org/10.62239/jca.2024.055

sample of 5% Cu content has the lowest Egap value, thus, it was chosen for the following characteristic analyses.

Energy-dispersive X-ray spectroscopy analyses

Energy-dispersive X-ray spectroscopy analysis (EDX) was performed to determine if the Cu-TiO_2 nanocrystals were incorporated into the SBA-16 mesoporous wall. The results revealed that the TiO_2-SBA-16 and 5%Cu-TiO_2-SBA-16 samples had a Si/Ti molar ratio around 30-35, over half the initial value (Si/Ti molar ratio=75). This fact suggests that TiO_2 nanocrystals and Cu-TiO_2 nanocrystals incorporated in the silica framework may replace the position of silanol groups during the synthesis procedure.

X-ray photoelectron spectra (XPS)

X-ray photoelectron spectra (XPS) is used to investigate the state of active species present on the materials. Fig. 2 (a-c) shows the XPS spectra obtained for TiO_2-SBA-16 and 5% Cu doped TiO_2-SBA-16, respectively.

The Ti 2p XPS results show two group peaks including Ti $2p_{3/2}$ and $2p_{1/2}$. The position of Ti $2p_{3/2}$ at 458.3 eV indicates the presence of Ti^{4+} oxidation state in octahedral coordination [19]. These results for Ti $2p_{3/2}$ indicate that Ti ions were in fact incorporated into the silica framework. The peaks at 932.4 eV and 952.9 eV are assigned to the Cu 2p core-level transition. The satellite peaks are also attributed to Cu^{2+}. The O1s spectrum shows two peaks at 529.9 eV and 533.9 eV. The former peak at 529.9 eV is similar to O^{2-} in CuO while the latter peak is assigned to oxygen bound from TiO_2 [20]. Thus, the XPS results show the formation of Ti^{4+} and Cu^{2+} ions in the SBA-16 framework.

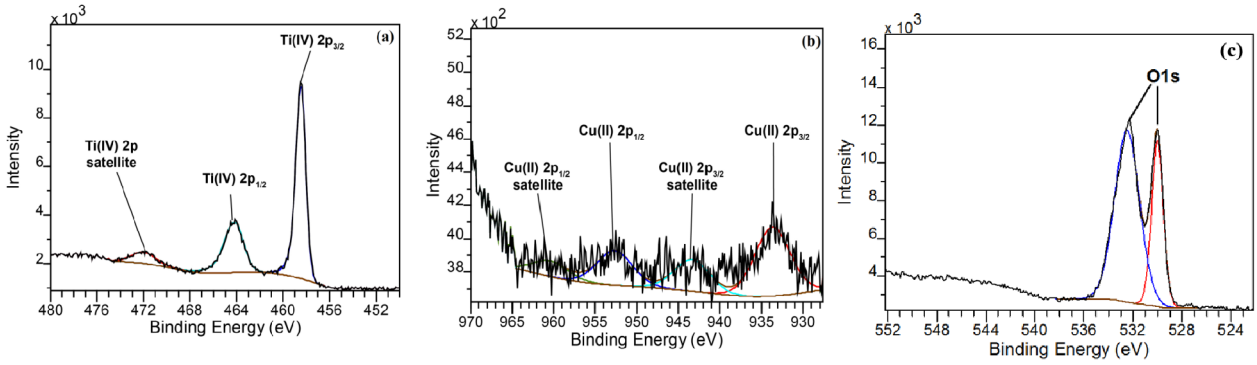

Fig. 2: XPS spectra of (a) Ti, (b) Cu, and (c) O of Cu-TiO_2-SBA-16 photocatalyst

N_2 adsorption/desorption analysis

The N_2 adsorption isotherms for prepared samples are shown in Fig. 3A.

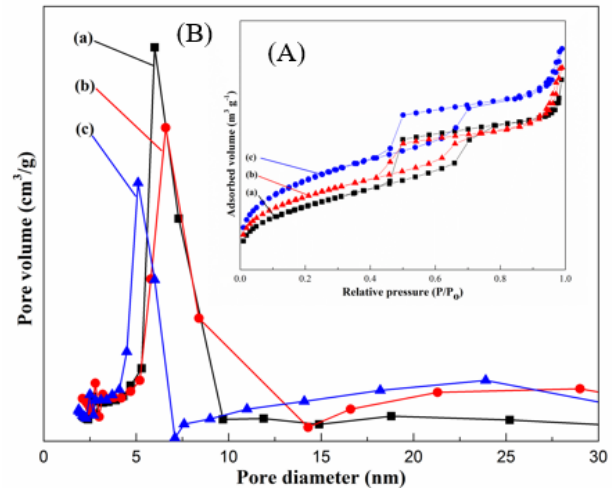

Fig. 3: (A) N_2 adsorption/desorption isotherms and (B) Pore size distribution curves of SBA-16 (a), TiO_2-SBA-16 (b), 5%Cu-TiO_2-SBA-16 (c).

For all samples, there are distinct capillary condensation steps at relative pressures (p/p) between 0.4 and 0.75, which indicates the presence of uniform mesopores. Moreover, all of the nitrogen adsorption–desorption isotherms belong to type IV with a H_2-type hysteresis loop, characteristic of materials with cage-like uniform mesopores interconnected by relatively narrow apertures, similar to SBA-16 materials. The surface areas and capillary volumes of the samples calculated by BET and BJH methods are shown in Table 1. It can be seen that the TiO_2-SBA-16 and 5%Cu-TiO_2-SBA-16 samples have higher surface area and pore volume than pure SBA-16. This may be due to the existence of TiO_2 and Cu-TiO_2 nanocrystals in the silica framework. Because the metal-oxygen bond is longer than the Si-O bond, incorporating metal complex molecules into the porous structure expands the framework parameters and cubic unit cell size. When Cu-TiO_2 was added, the cubic structure with an estimated capillary diameter in the range of 5.3-5.4 nm was maintained.

https://doi.org/10.62239/jca.2024.055

Table 1: Textural and structural characteristics of samples

Samples	S_{BET} (m^2g^{-1})	S_{micro} (m^2g^{-1})	V_{pore} (cm^3g^{-1})	D_p (nm)	d_{110} (nm)	a_0 (nm)
SBA-16	809.8	335.5	0.158	5.31	12.15	14.03
TiO_2-SBA-16	1033.7	518.3	0.239	5.34	11.74	13.55
5%Cu-TiO_2-SBA-16	904.5	363.6	0.161	5.33	11.26	13.00

Transmission electron microscopy (TEM)

TEM images of pure SBA-16, TiO_2-SBA-16 and Cu-TiO_2-SBA-16 are shown in Fig. 4 (a-c), respectively.

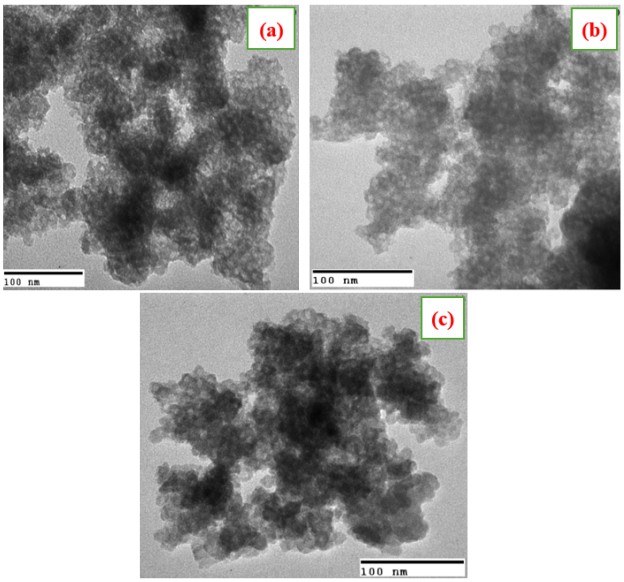

Fig. 4: TEM images of (a) pure SBA-16, (b) TiO_2-SBA-16 and (c) 5%Cu-TiO_2-SBA-16.

As seen in Fig 6 (a-c), material is highly ordered with the cubic mesostructure. The cubic Im3m can be seen in all pure SBA-16 and Cu-TiO_2-SBA-16 samples, which indicates that the mesoporous structure of SBA-16 was not destroyed after incorporation of the metals complex . Fig 6-b and c have a presence of black spots which may be due to the metal nanocrystals incorporated inside the mesoporous. These results reinforce the ordered cubic mesoporous of material obtained from the above XRD results. The uniform pore size is in good agreement with the value measured from N_2 adsorption–desorption experiments. These pores allow rapid diffusion of various liquid reactants and products during photocatalytic reaction.

Catalytic activity

The Cu-TiO_2-SBA-16 catalyst was tested in the oxidative desulfurization (ODS) process using 30% H_2O_2 solution as the oxidant at different reaction temperatures and the optimal temperature to perform the reaction for the highest conversion of DBT was 70°C, the sulfur removal reaction efficiency achieved the best value (Fig. 5).

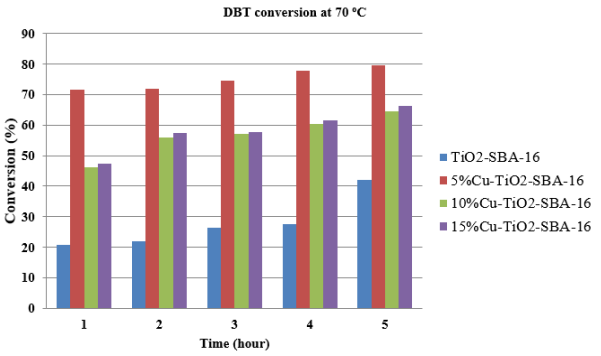

Fig. 5: The conversion of DBT with different photocatalysts.

At high temperature, the generation rate of hydroxyl radicals was at an optimum and the interfacial electron-transfer kinetics were improved. Therefore, the photocatalytic activity of catalysts was increased slightly, which provides higher sulfur removal efficiency. These results suggested that the DBT photocatalytic degradation reaction followed pseudo first-order kinetics, meaning increasing of temperature leads to increasing reaction efficiency.

The results show that TiO_2-SBA-16 has low photocatalytic activity with very small DBT conversion. However, the photocatalytic activity of Cu-TiO_2-SBA-16 samples increased in the following order: 15%Cu-TiO_2-SBA-16<10%Cu-TiO_2-SBA-16<5%Cu-TiO_2-SBA-16. TiO_2 is a photocatalyst that absorbs ultraviolet light with wavelengths shorter than 390 nm. The electrons in the TiO_2 valence band are excited and move to the conduction band under UV irradiation. Then, ·OH radicals and photogenerated holes form and decompose organic compounds. However, the high recombination rate of photogenerated carriers leads to low photoactivity of pure TiO_2. When CuO species are introduced into TiO_2 samples, CuO particles can act as electron traps, promoting electron hole separation and then transferring the trapped electron to the adsorbed O_2, which acts as an electron acceptor on TiO_2 surface. The holes remain in the TiO_2 valence band after the excited electrons move. Therefore, the recombination

https://doi.org/10.62239/jca.2024.055

of electron-hole pairs is limited and the photocatalytic reaction can be significantly enhanced. Besides, the formation of sulfoxide products from DBT conversion is as follows: in the Cu-TiO_2-SBA-15 photocatalyst, the reaction occurs between titanium and the electron pair of oxygen of hydrogen peroxide to form titanium-peroxo complex. These complexes then undergo nucleophilic addition reaction by sulfur atom of DBT to produce sulfoxide products [33]. The presence of copper ions (Cu_xO) replacing titanium sites leads to a lower band gap energy compared to TiO_2 pure, resulting in electrons easily migrate from the valence band to the conduction band in Cu-TiO_2-SBA-16 photocatalyst, which increases conversion efficiency of DBT.

4. Conclusion

In summary, TiO_2 and Cu-TiO_2 nanocrystals were incorporated into the mesoporous silica framework of SBA-16. The results obtained by X-ray diffraction and nitrogen adsorption-desorption isotherms confirmed that the photocatalytic samples retained their structure and support properties after synthesis, while the results XPS demonstrated the presence of metal complexes in the pores of SBA-16. The incorporation of metal complexes causes an increase in specific surface area, pore volume and pore diameter. Furthermore, Cu-TiO_2 samples showed enhanced UV harvesting compared to TiO_2. Liquid-phase oxidation reactions of DBT with hydrogen peroxide as oxidant were carried out with these catalysts. The results show that 5%Cu-TiO_2-SBA-16 has the highest photocatalytic activity and may have potential applications in related fields.

Acknowledgement

The authors gratefully acknowledge the financial support of National Foundation for Science and Technology Development (Nafosted), Code 105.99-2023.01.

References

1. X.B. Lim, W.-J. Ong, Nanoscale Horiz.6 (2021) 588–633. https://doi.org/10.1039/D1NH00127B
2. D. Julião, S. Ribeiro, B. De Castro, L. Cunha-Silva, Balula SS. Hershey, PA, USA: IGI Global; 2016. p. 426–58. https://doi.org/10.4018/978-1-4666-9545-0.ch014
3. V.C. Srivastava, RSC Adv 2 (2012) 2, 759–83. https://doi.org/10.1039/C1RA00309G
4. U.S. Environmental Protection Agency, Diesel Fuel Standards and Rulemakings, https://www.epa.gov/diesel-fuelstandards/ diesel-fuel-standards standards-and-rulemakings, 2020.
5. X. Weng, L. Cao, G. Zhang, F. Chen, L. Zhao, Y. Zhang, J. Gao, C. Xu, Ind. Eng. Chem. Res. 59 (2020) 59, 21261–21274. https://doi.org/10.1021/acs.iecr.0c04049.
6. M.A. Betiha, A.M. Rabie, H.S. Ahmed, A.A. Abdelrahman, M.F. El-Shahat, Egypt. J. Pet. 27 (2018) 715–730. https://doi.org/10.1016/j.ejpe.2017.10.006.
7. K.X. Lee, J.A. Valla, React. Chem. Eng. 4 (2019) 1357–1386. https://doi.org/10.1039/C9RE00036D.
8. P. Sikarwar, V. Gosu, V. Subbaramaiah, Rev. Chem. Eng. 35 (2019) 669–705. https://doi.org/10.1515/revce-2017-0082.
9. M.H. Ibrahim, M. Hayyan, M.A. Hashim, A. Hayyan, Renew. Sustain. Energy Rev. 76 (2017) 1534–1549.
10. B.K. Mutuma, G.N. Shao, W.D. Kim, H.T. Kim, J. Colloid Interface Sci. 442 (2015) 1–7. https://doi.org/10.1016/j.jcis.2014.11.060.
11. D.I. Anwar, D. Mulyadi, Procedia Chem. 17 (2015) 49–54. https://doi.org/10.1016/j.proche.2015.12.131.
12. T. Sreethawong, S. Yoshikawa, Catal. Commun. 6 (2005) 661–668. https://doi.org/10.1016/j.catcom.2005.06.004.
13. U.G. Akpan, B.H. Hameed, Appl. Catal. A: Gen. 375 (2010) 1–11. https://doi.org/10.1016/j.apcata.2009.12.023.
14. X.N. Pham, T.D. Pham, B.M. Nguyen, H.T. Tran, D.T. Pham, J. Chem. 2018 (2018) ID 8418605. https://doi.org/10.1155/2018/8418605.
15. X.N. Pham, B.M. Nguyen, H.T. Thi, H.V. Doan, Adv. Powder Technol. 29 (8) 2018, 1827-1837. https://doi.org/10.1016/j.apt.2018.04.019.
16. X.N. Pham, M.B. Nguyen, H.S. Ngo, H.V. Doan, J. Ind. Eng. Chem. 90 (2020) 358-370. https://doi.org/10.1016/j.jiec.2020.07.037
17. E.M. Rivera-Muñoz, R. Huirache-Acuña. Int. J. Mol. Sci. 11 (2010) 3069-3086. https://doi.org/10.3390/ijms11093069.
18. A. Kumar, D. Srinivas, J. Mol. Catal. A: Chem. 368– 369 (2013) 112–118. https://doi.org/10.1016/j.molcata.2012.11.026
19. X.N. Pham, M.B. Nguyen, H.V. Doan, Adv. Powder Technol. 31(8) (2020) 3351-3360. https://doi.org/10.1016/j.apt.2020.06.028.
20. A. Adamu, M. Isaacs, K. Boodhoo, F.R. Abegão, J. CO2 Util. 70 (2023) 102428. https://doi.org/10.1016/j.jcou.2023.102428.
21. Q. Liu, T. Su, H.Zhang, W. Liao, W. Ren, Z. Zhu, K. Yang, C. L en, J. Yu, D. Zhao, H. Lü. Fuel 333 (2023) 126286. https://doi.org/10.1016/j.fuel.2022.126286.
22. Z. Song, M. Bi, J. Li, Y. Guo, Q. Xu, Y. He, N. Zhao, L. Chen, D. Ren. Silicon 16 (2024) 4159–4172. https://doi.org/10.1007/s12633-024-02982-1